ENVIRONMENTAL ENGINEERING SCIENCE
Volume 36, Number 4, 2019

DOI: 10.1089/ees.2018.0278

Magnetically Separable Fe_3O_4/BiOBr Microspheres: Synthesis, Characterization, and Photocatalytic Performance for Removal of Anionic Azo Dye

J ,[1] - ,[1,*] - o J ,[1] o - ,[1] -M o ,[1]
J - ,[2] G -M [3]

[1]Department of Environmental Engineering, Taizhou University, Taizhou, P.R. China.
[2]Environmental Engineering Program, University of Northern British Columbia, Prince George, Canada.
[3]Key Laboratory of Environmental Biology and Pollution Control (Hunan University), Ministry of Education, Changsha, P.R. China.

Received: June 25, 2018 *Accepted in revised form: October 19, 2018*

Abstract

Recyclable magnetic Fe_3O_4/BiOBr microspheres (m-Fe_3O_4/BiOBr MSs) were synthesized by a simple solvethermal method. The crystals' optical, morphology, and magnetic properties of m-Fe_3O_4/BiOBr MSs were characterized using X-ray diffraction, scanning electron microscopy, transmission electron microscopy, energy dispersive analysis of X-rays, UV–vis diffuse reflectance spectroscopy, Brunauer–Emmett–Teller, and vibrating sample magnetometry techniques. An anionic dye, Congo red (CR), was selected as a model pollutant to evaluate the photocatalytic activity of m-Fe_3O_4/BiOBr MSs under simulated solar light irradiation. By calculation, the pseudo-first-order rate constant for photocatalytic degradation of CR was 0.0011 and 0.0046 min^{-1} using pure BiOBr MSs and m-Fe_3O_4/BiOBr MSs, respectively. Enhanced photocatalytic activity of m-Fe_3O_4/BiOBr MSs can result from superior adsorption and transfer performance to organic contaminants in aqueous system. Both the h^+ radicals and $O_2^{\square-}$ radicals were main active species that drive the photocatalytic decolorization of CR solution by m-Fe_3O_4/BiOBr MSs. Furthermore, the m-Fe_3O_4/BiOBr MSs can be easily recovered and recycled after the treatment process because of the presence of magnetic Fe_3O_4. This work suggests that m-Fe_3O_4/BiOBr MSs may be a promising photocatalyst for photocatalytic treatment of organic wastewater and other environmental remediation.

Keywords: BiOBr; congo red; decolorization; Fe_3O_4; magnetic separation; photocatalysis

Introduction

DYE TUFF ARE WIDELY U ED in textile, dye synthesis, pharmaceuticals, cosmetics, and electroplating and are serious contaminants due to the toxicity and potentially carcinogenic nature of these substances (Huo *et al.*, 2013). Several techniques have been reported and used for removing dyes from water in wastewater treatment plants, such as adsorption (Zhu *et al.*, 2011; Wen *et al.*, 2016), advanced oxidation processes (Ahmed *et al.*, 2011; Yu *et al.*, 2013), biological and electrochemical (Brillas and Martínez-Huitle, 2015). However, synthetic dyes could be difficult to be eliminated from wastewater by conventional biological techniques owing to their low biodegradability and stable aromatic structure.

Adsorption is one of the most effective dye-removal methods in aqueous systems; this process transports dyes from aqueous solution to solid phase (adsorbents) rather than causing their degradation (Zhu *et al.*, 2011). In addition, to treat effectively dye-containing wastewater, various kinds of semiconductor materials, such as TiO_2, ZnO, and their composites (Panthi *et al.*, 2015; Lee *et al.*, 2016), have been developed. Unfortunately, the low visible light response or difficulty of recycling limits the practical use of those photocatalysts. Therefore, exploiting novel, high-efficient, and eco-friendly methods are necessary for effective purification and treatment of dye-containing wastewater (Ahmed *et al.*, 2011; Zhu *etl.* , 2016).

Bismuth oxyhalides(BiOX, X =Cl,Br, I) used for effective degradation of organic pollutants due to its nontoxicity, high stability, suitable energy, relatively superior visible light photocatalytic ability,and others.Li *et al.*, 2016; Si *et al.*, 2016; Zhao *et al.*, 2016; Mera *et al.*,2017). Over the last decade, the controllable synthesis and selective assembly of BiOBr nanobeltsLi nonflakes,Yu *et al.*, 2013; *et al.*, 2015), microspheres Qiang *et al.*, 2016; Mera *et al.*, 2017), and nanoflowers (Huo *et al.*, 2012) have been developed by all kinds of methods.

*Corresponding author: Department of Environmental Engineering, Taizhou University, No. 1139, Municipal Government Avenue, Taizhou, Zhejiang 318000, P.R. China. *Phone:* +86 1835860 9860, *Fax:* +86 576 8866 0328, *e-mail:* zhuhaoedu@126.com

Those BiOBr showed excellent photocatalytic activity for the decolorization and degradation of an azo dye under visible light or simulated solar light. However, the applications of most of these nanoscale BiOBr materials have seriously been inhibited by the difficulty in recovery and recycling after photocatalytic treatment due to their relatively small size.

Immobilizing photocatalysts on magnetic substrates by some feasible methods is proven to be an effective approach for removing and recycling particles. Owing to their high super-magnetism, magnetic Fe_3O_4 nanoparticles have caused increasing attention for easy separation and fast recovery (Polshettiwar *et al.*, 2011; Linley *et al.*, 2013; Idris *et al.*, 2014; Li *et al.*, 2015; Lin *et al.*, 2015; Gao *et al.*, 2017; Zhu *et al.*, 2017). In addition, it has been reported that Fe_3O_4 nanoparticles produce electron-hole pairs easily under visible light irradiation and could enhance further photocatalytic activity by suppressing the recombination of photogenerated carriers since they could act as an electron-transfer channel and acceptor (Idris *et al.*, 2014; Li *et al.*, 2015).

Hence, it can be foreseen that the incorporation of the magnetite nanocrystals Fe_3O_4 into BiOBr not only can recycle the photocatalyst by simple magnetic separation under an external magnetic field, but also can offer some synergetic enhancement of the photocatalytic activity, which is very attractive for photocatalytic treatment of dye-containing wastewater.

To the best of our knowledge, there are few studies on the degradation of anionic azo dye by recyclable magnetic Fe_3O_4/BiOBr microspheres (m-Fe_3O_4/BiOBr MSs) under simulated solar light irradiation. Congo red (CR) dye (sodium salt of benzidinediazo-bis-1-naphtylamine -4-sulfonic acid) (C.I. No. 22120) is one of the most important anionic azo dyes used for dyeing cotton in textile industries and also in wood pulp and paper industries.

In this study, recyclable magnetic m-Fe_3O_4/BiOBr MSs were successfully prepared by a simple solvethermal method. The microstructure, morphology, optical, and magnetic properties of the resultant samples were characterized using X-ray diffraction (XRD), energy dispersive analysis of X-rays (EDX), scanning electron microscopy (SEM), transmission electron microscopy (TEM), UV–vis diffuse reflectance spectroscopy (DRS), Brunauer–Emmett–Teller (BET), and vibrating sample magnetometry (VSM) techniques. The photocatalytic activity of m-Fe_3O_4/BiOBr MSs was evaluated by photocatalytic degradation of CR solution under simulated solar light irradiation. The influences of operational parameters such as initial CR concentration, photocatalyst dosage, and successive cycles on the degradation reaction were studied. Moreover, the roles of reactive species (h^+, $\cdot O_2^-$ and $\cdot OH$) and the possible mechanism of photocatalytic activity enhancement were studied in detail.

Materials and Methods

Materials

CR dye used as a model anionic azo dye was purchased from Yongjia Fine Chemical Factory (Wenzhou, China). The chemical structure of CR dye is shown in Fig. 1. Titanium dioxide (P25) with purity of at least 99.5% was obtained from Degussa. A commercial anatase TiO_2 (a-TiO_2, purity >99.7%) was purchased from Xiamen Micaren Technology Co., Ltd. (Xiamen, China). $Bi(NO_3)_3 \cdot 5H_2O$, KBr, $FeCl_3 \cdot 6H_2O$, $FeSO_4 \cdot 7H_2O$, $NH_3 \cdot H_2O$ (28%, v/v), and ethylene glycol were purchased from Shanghai Chemical Reagent Research Institute (Shanghai, China) and used as received. All chemicals were analytical grade and used without further purification.

Synthesis of magnetic Fe_3O_4 nanoparticles

Fe_3O_4 nanoparticles were prepared by hydrothermal co-precipitating Fe^{2+} and Fe^{3+} salts under the presence of N_2 gas (Zhu *et al.*, 2011). Thirty millimolar of $Fe(NO_3)_3 \cdot 9H_2O$ and 15 mmol of $FeSO_4 \cdot 7H_2O$ were dissolved in 45 mL of deoxygenated distilled water. Chemical co-precipitation was achieved under vigorous stirring in a water bath at 313 K for 30 min by adding 40 mL of $NH_3 \cdot H_2O$ solution (28%, v/v) in the protection of N_2 gas. The temperature of solution was adjusted and maintained at 333 K for another 5 h while adding another 6.6 mL of $NH_3 \cdot H_2O$ solution during the reaction. After reaction, Fe_3O_4 nanoparticles were magnetically separated from aqueous solution by an adscititious magnet at room temperature, and washed three times with water and ethanol, and finally dried in a vacuum oven at 343 K until constant weight.

Synthesis of magnetic m-Fe_3O_4/BiOBr MSs

The m-Fe_3O_4/BiOBr MSs were synthesized by a simple solvothermal method, as illustrated in Fig. 2. Three millimolar of $Bi(NO_3)_3 \cdot 5H_2O$ and 3 mmol of KBr were initially dissolved in 60 mL ethylene glycol and sonicated for 0.5 h at room temperature. Then, 3 mmol of as-prepared magnetic Fe_3O_4 nanoparticles were dispersed into the resulting solution. After vigorously stirring for another 40 min, the obtained suspension was transferred into a 100 mL Teflon-lined

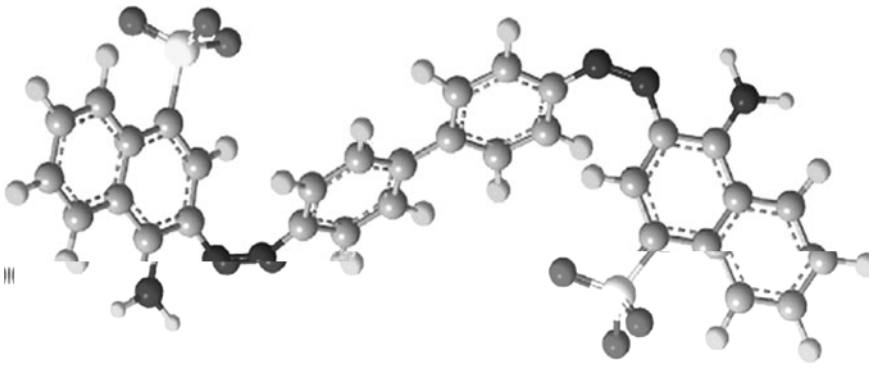

FIG. 1. Chemical structure of CR. CR, Congo red.

stainless steel autoclave and heated to 433 K with a heating ramp of 2 K/min for 12 h. After the reaction was completed, the sample was cooled down naturally, separated from the mixture system by applying an external magnetic field, and washed with distilled water and ethanol several times, respectively, with the aid of ultrasonic technique. Slight ultrasonic process is conducive to the effective diffusion of chemical reagents, thus improving the cleaning effect. The product was finally dried under at 333 K for 12 h. For comparison, pure BiOBr MSs were prepared by previous proce-

temperature was maintained at 293 K by using cooling water system. The initial concentration of CR was 20 mg/L and the photocatalyst dosage was 1.0 g/L. After a given irradiation time, 3 mL of the suspension was withdrawn. The photocatalyst was separated from the mixture system by applying an external magnetic field. The concentration of CR solution was analyzed by measuring its characteristic absorption peak ($\lambda_{max} = 496$ nm) with a UV–vis spectrophotometer (Beijing Purkinje General Instrument Co., Ltd., China). The concentration of CR dye was calculated by a standard calibration curve obtained from the absorbance of the dye at different known concentrations. For the convenience of comparison,

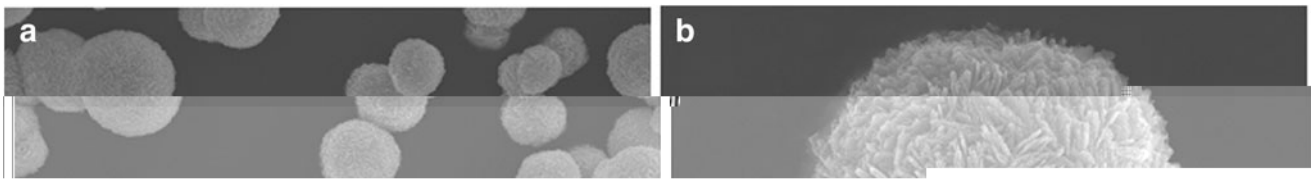

FIG. 4. Scanning electron microscopy images of BiOBr **(a**, **b)**, m-Fe_3O_4/BiOBr MSs **(c**, **d)**, energy-dispersive X-ray spectroscopy spectra of BiOBr **(e)**, and m-Fe_3O_4/BiOBr **(f)**.

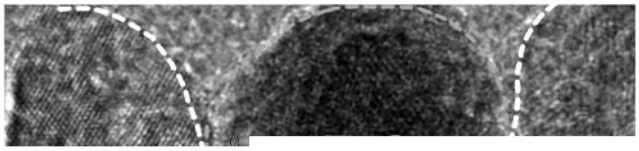

FIG. 5. High resolution transmission electron microscope image of m-Fe_3O_4/BiOBr MSs.

commercial TiO_2 that is, Degussa P-25 TiO_2 (P25) and commercial a-TiO_2 (purity >99.7%) were used to treat CR solution under the same conditions.

Photocatalytic degradation efficiency (η%) of CR solution by m-Fe_3O_4/BiOBr MSs was calculated according to Equation (1)

$$\eta \frac{(C_0 - C_t)}{C_t} \times 100\% \quad (1)$$

where C_0 is the initial concentration of CR (mg/L), and C_t is the instant concentration of dye at time t (mg/L),

When initial concentration of pollutant is lower, a simplified Langmuir–Hinshelwood (L–H) kinetic model can be used to describe photocatalytic CR degradation [Eq. (2)] (Zhu *et al.*, 2009).

$$\ln\left(\frac{C_0}{C_t}\right) k_{app} t \quad (2)$$

where k_{app} is the apparent first-order rate constant (min^{-1}). A plot of $\ln(C_0/C_t)$ versus t will yield a slope of k_{app}.

Results and Discussion

Characterization of as-prepared samples

X-ray diffraction. The crystal phase and crystal structure of as-prepared samples were determined by XRD. Figure 3 presents the XRD patterns of the Fe_3O_4, BiOBr, and m-Fe_3O_4/BiOBr MSs. The diffraction peaks at 30.23°, 35.64°, 43.38°, 53.80°, 57.31°, and 62.86°, can be assigned to the (220), (311), (400), (422), (511), and (440) crystal planes of pure Fe_3O_4 with a cubic spinel structure, respectively (JCPDS card no. 65-3107) (Zhi *et al.*, 2006; Zhu *et al.*, 2011). As for pure BiOBr, the reflections are consistent with the standard pattern of a tetragonal phase BiOBr (JCPDS Card No. 78-0348), and the main diffraction peaks at about 25.19°, 32.24°, 39.3°, 46.25°, 50.7°, 53.4°, and 57.17° can be indexed to the (101), (110), (112), (200), (104), (211), and (212) planes of the tetragonal BiOBr, respectively (Xue *et al.*, 2014; Liu *et al.*, 2015). In the diffraction patterns of m-Fe_3O_4/BiOBr MSs shown in Fig. 3, both the tetragonal BiOBr phase and cubic Fe_3O_4 phase were detected, indicating that both Fe_3O_4 and BiOBr have been coupled together.

SEM and TEM. The morphology and microstructure of BiOBr MSs and m-Fe_3O_4/BiOBr MSs were investigated by SEM. Figure 4a shows that the as-prepared BiOBr MSs possess almost the similar three-dimensional (3D) microsphere morphology with a large diameter of approximately 1.60–3.0 μm. As can be seen from the high-magnification SEM images (Fig. 4b), the entire 3D BiOBr MSs were self-assembled by numerous nanosheets with a thickness ranged from 10 to 35 nm. The nanosheets are aligned from the center of the microsphere to the surface, and give a floral appearance (Chen *et al.*, 2011). The microstructure of the m-Fe_3O_4/BiOBr MSs is shown in Fig. 4c. The m-Fe_3O_4/BiOBr MSs possessed much bigger size than that of the pure BiOBr MSs. Fe_3O_4 nanoparticles were observed to be mingled among the BiOBr nanosheets or adhered to the BiOBr MSs surface, which could facilitate magnetic separation of m-Fe_3O_4/BiOBr MSs (Fig. 4d). Additionally, the chemical composition of as-prepared BiOBr MSs and m-Fe_3O_4/BiOBr MSs were also detected by EDX. The BiOBr MSs contained

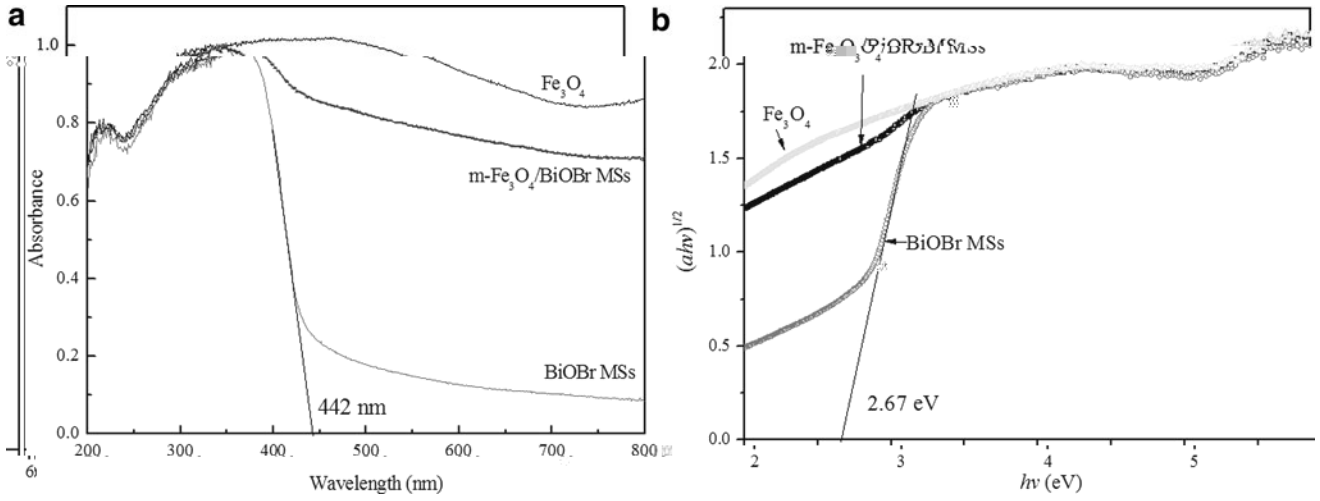

FIG. 6. UV–vis diffuse reflectance spectra **(a)** and the plot of $(\alpha hv)_{0.5}$ versus energy (hv) **(b)** of Fe_3O_4, BiOBr MSs, and m-Fe_3O_4/BiOBr MSs.

elements of Bi, Br, and O (Fig. 4e), while the major constituents for m-Fe_3O_4/BiOBr MSs were Fe, O, Bi, and Br (Fig. 4f). The peaks of Bi, Br, and O were mainly generated by BiOBr MSs while the peaks of Fe and O resulted from magnetic Fe_3O_4. These results were consistent with the XRD data (Fig. 3).

After the introduction of Fe_3O_4 into BiOBr MSs, the presence of Fe_3O_4 nanoparticles was also confirmed by HRTEM image of m-Fe_3O_4/BiOBr MSs (Fig. 5), which showed that sphere Fe_3O_4 nanoparticle was embedded between the BiOBr nanosheets. The close incorporation of Fe_3O_4 with BiOBr MSs can not only enhance the visible light photocatalytic performance of m-Fe_3O_4/BiOBr MSs, but also enhance the photostability by inhibiting the photocorrosion.

Diffuse reflectance spectroscopy. It is well known that photocatalytic activity is closely related to the optical absorbance ability and the migration of photo-generated electron-hole (e^-/h^+) pairs. The UV-Vis DRS of Fe_3O_4, BiOBr MSs, and m-Fe_3O_4/BiOBr MSs are shown in Fig. 6. As can be seen, pure BiOBr MSs show absorbance in visible range with an absorption edge about at 442 nm (Fig. 6a) and have a band gap of 2.67 eV (Fig. 6b) according to the equation $\alpha h\nu = A(h\nu - Eg)^{n/2}$ (Zhang *et al.*, 2015a, 2015b). Compared with TiO_2, which has a band gap energy of ca. 3.2 eV (anatase), the smaller band gap energy of BiOBr makes it more easier to be activated by visible light or solar light (Zhang *et al.*, 2015a, 2015b). The absorbance intensity of Fe_3O_4 is very strong in both visible range and UV region from 200 to 800 nm, which results from the black appearance of pure Fe_3O_4. As a result, the absorbance ability of m-Fe_3O_4/BiOBr MSs in the visible range increased due to the strong visible light response of Fe_3O_4. The considerable absorbance of m-Fe_3O_4/BiOBr MSs in the visible region implies the possibility of high photocatalytic activity for the photodecolorization of CR solution under simulated solar light irradiation.

Specific surface areas and N_2 adsorption–desorption isotherms. The specific surface area and porosity of as-prepared pure BiOBr and m-Fe_3O_4/BiOBr MSs were investigated by using N_2 adsorption–desorption isotherms. As

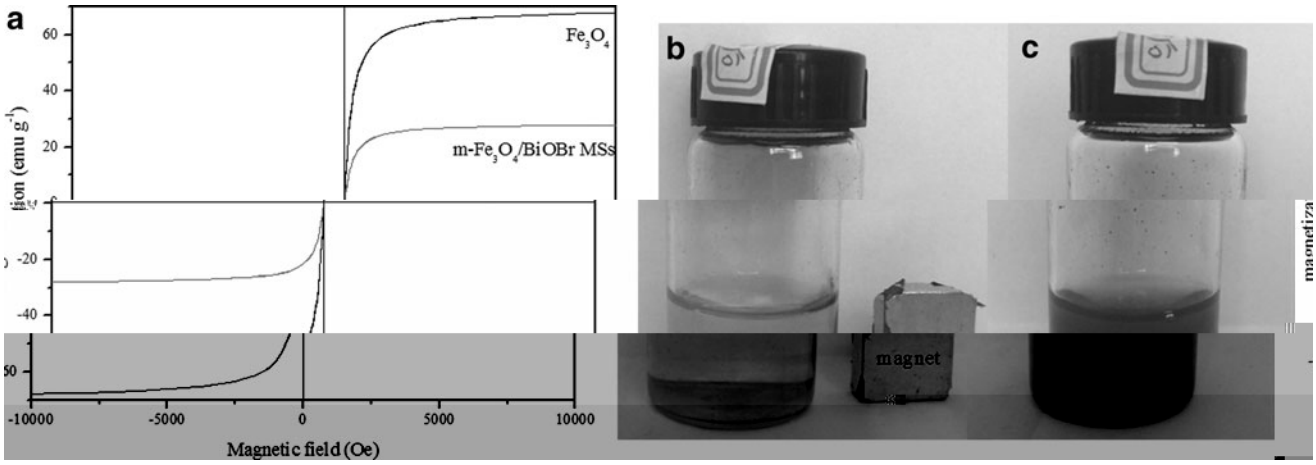

FIG. 8. Room-temperature magnetization curves **(a)** of Fe_3O_4 and m-Fe_3O_4/BiOBr MSs and the magnetic separation **(b)** and redispersion **(c)** of m-Fe_3O_4/BiOBr MSs.

similar to some values reported in other literatures (Zhi *et al.*, 2006). For the m-Fe_3O_4/BiOBr MSs, the saturation magnetization reached 27.89 emu/g. Although the saturated magnetization of m-Fe_3O_4/BiOBr MSs decreased due to the presence of nonmagnetic BiOBr MSs, it was still higher than those of many reported magnetic photocatalysts, such as Fe_3O_4:TiO_2 core-shell Nanoparticles (5.94 emu/g) (He *et al.*, 2008), P25–graphene–Fe_3O_4 nanocomposite (5.276 emu/g) (Cheng *et al.*, 2016), Fe_3O_4/g-C_3N_4 (16.80 emu/g) (Zhi *et al.*, 2016), Ag/Fe_3O_4/g-C_3N_4 (12.68 emu/g) (Zhi *et al.*, 2016), and Cu_2O/CS–Fe_3O_4 (15.1 emu/g) (Cao *et al.*, 2015). The m-Fe_3O_4/BiOBr MSs were separated fleetly from treated solution and collected to the sidewall of a cuvette after 5 s using an ordinary magnet (Fig. 8b), suggesting that m-Fe_3O_4/BiOBr MSs have an excellent magnetic responsivity. What is more, the m-Fe_3O_4/BiOBr MSs can be redispersed in aqueous solution by vigorous shaking once the magnetic field is removed (Fig. 8c), resulting in a black-colored suspension. These results show that m-Fe_3O_4/BiOBr MSs possess excellent magnetic responsivity and redispersibility simultaneously, which are important for practical reuse of m-Fe_3O_4/BiOBr MSs.

Adsorption behavior and photocatalytic activity

Figure 9a shows normalized change in concentration of CR dye under different experiment conditions. The adsorption of CR on BiOBr MSs and m-Fe_3O_4/BiOBr MSs were carried out with different period of contact time in the range of 0–240 min, as shown in Fig. 9a. As it is evident from Fig. 9a, BiOBr MSs attained adsorption saturation at 30 min while adsorption of CR on Fe_3O_4/BiOBr MSs was relatively slow and did not reach adsorption saturation even at 240 min. The adsorption capacities for CR dye on BiOBr MSs and Fe_3O_4/BiOBr MSs for 240 min of contact time were found to be 4.99 and 10.19 mg/g, respectively (Fig. 9b), indicating that m-Fe_3O_4/BiOBr MSs possessed higher adsorption capacity for effectively removing CR azo dye from aqueous solution. Since the photo-oxidation reaction usually takes place on the photocatalysts surface, higher equilibrium adsorption capacity is very important and favorable for the photocatalytic treatment of organic pollutants (Zhu *et al.*, 2012). Due to higher correlation coefficient values ($R^2 > 0.99$) and closer values between experimental and calculated theoretical adsorption capacities (q_e), the pseudo-second-order model was considered as the fitting model in describing the CR adsorption on both BiOBr MSs and m-Fe_3O_4/BiOBr MSs (Fig. 9c). It suggested that the rate-limiting step of CR adsorption on both BiOBr MSs and m-Fe_3O_4/BiOBr MSs might be chemical adsorption (Wen *et al.*, 2016).

Photocatalytic activity of BiOBr and m-Fe_3O_4/BiOBr MSs was also studied, as shown in Fig. 9a. After irradiation of 240 min, the photocatalytic decolorization efficiency is 35.81% and 77.52% for BiOBr MSs and m-Fe_3O_4/BiOBr MSs respectively. It is seen that the m-Fe_3O_4/BiOBr MSs exhibited higher degradation efficiency than BiOBr MSs. For the convenience of comparison, two kinds of commercial TiO_2, that is, Degussa P-25 TiO_2 (P25) and commercial a-TiO_2 (purity >99.7%) were used to treat CR solution under the same conditions. The removal efficiency of CR by P25 and a-TiO_2 is calculated to be 43.52% and 16.83%, respectively, which is lower than that by m-Fe_3O_4/BiOBr MSs. It is well known that P25 has excellent photocatalytic activity under UV light (Reza *et al.*, 2017). As a result, m-Fe_3O_4/BiOBr MSs are a good alternative to treat organic pollutant in aqueous solution under simualted solar light.

According to previous studies (Zhu *et al.*, 2009), photocatalytic process can be expressed by the L–H model. The corresponding apparent first-order rate constant (k_{app}) was calculated from photocatalytic reaction and the calculated values are 0.0011 and 0.0046 min^{-1} for BiOBr MSs and m-Fe_3O_4/BiOBr MSs respectively. The k_{app} constant of m-Fe_3O_4/BiOBr MSs (0.0046 min^{-1}) was found to be about 4.18 times that of BiOBr (0.0011 min^{-1}). This enhanced degradation may be due to the synergistic effect of the adsorption and photocatalysis. As we can see from Fig. 9d, the intensity of the absorption peak at 496 nm of CR decreased with increasing irradiation time and red color of the reaction solution nearly converted into colorless.

Effect of initial CR concentration and catalyst dosage on decolorization

From an application point view, it is important to study the dependence of degradation on the initial concentration of

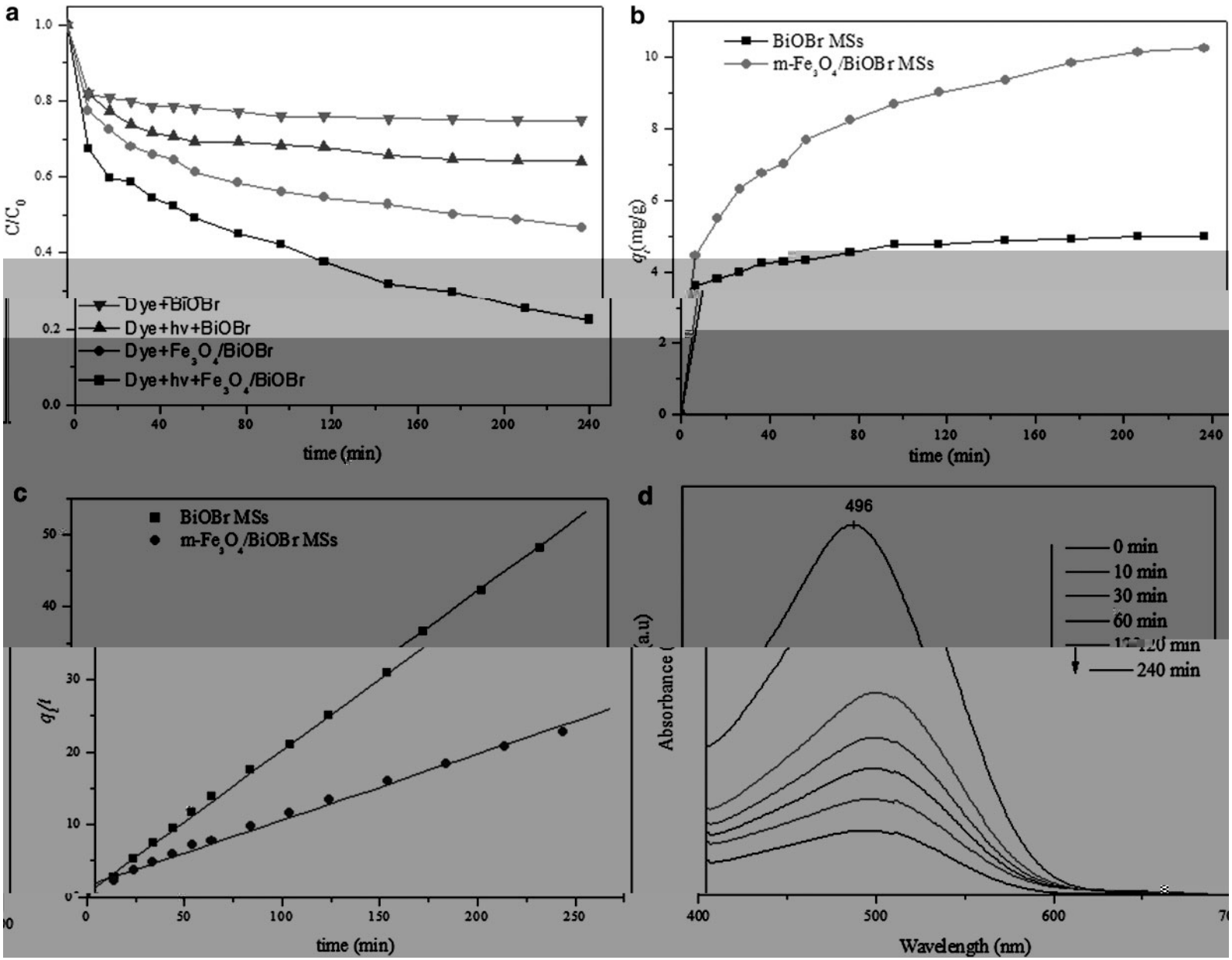

FIG. 9. Effect of contract time by BiOBr and m-Fe_3O_4/BiOBr MSs: different experiment conditions **(a)**, adsorption capacities **(b)**, pseudo-second-order model **(c)** and UV–vis absorption spectra of CR solution **(d)**.

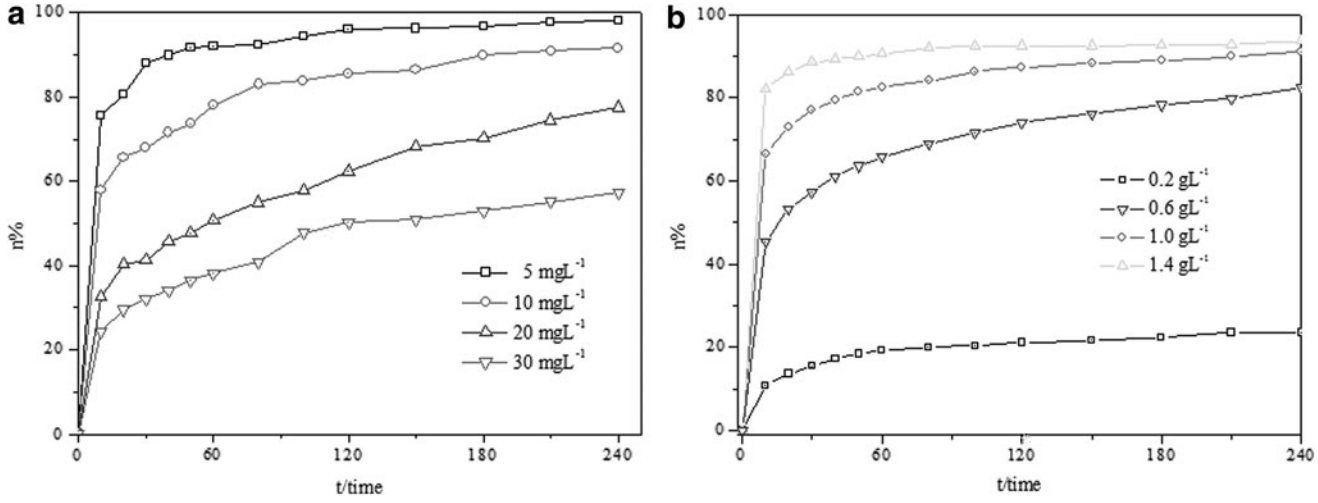

FIG. 10. Effects of CR initial concentration **(a)** and m-Fe_3O_4/BiOBr MSs dosage **(b)** on CR decolorization efficiency.

pollutant and the photocatalyst dosage. The increase in initial dye concentration from 5 to 30 mg/L decreased the degradation rate constants from 0.024 to 0.004 min^{-1}. The possible explanation for this behavior is that as the CR initial concentration increases, the path length of the photons entering the solution decreases. This may lead to the decrease in photocatalytic degradation efficiency. The effect of photocatalyst dosage on CR decolorization was studied by varying the catalyst dosage from 0.2 to 1.4 g/L for 20 mg/L CR aqueous solutions. The results are presented in Fig. 10b. The results indicated that the decolorization of CR was influenced by the catalyst dosage and CR decolorization rate increased with increasing catalyst dosage. When the m-Fe_3O_4/BiOBr MSs concentration was 0.1 g/L, only 23.56% of CR was degraded after 4 h irradiation, but 91.18% of CR could be degraded when the photocatalyst dosage reached 1.4 g/L. When a small amount of catalyst was dispersed in the reaction medium, all surface active sites were available. Accordingly, the decolorization rate increased with the increase of catalyst dosage. The addition of catalyst amount above 1.0 g/L would have a slight increase in efficiency, while there was increased turbidity/opacity of the reaction suspension and decreased transmission through the suspension due to excess catalyst particles.

Stability of photocatalyst

It is well known that stability and reusability of photocatalysts is very important for practical application because its use for longer period of time leads to a significant cost reduction of the practical treatment. To investigate the stability and reusability of the magnetic m-Fe_3O_4/BiOBr MSs, three successive CR photodegradation experiments were carried out under simulated solar light irradiation and the results are shown in Fig. 11. As shown in Fig. 8b, m-Fe_3O_4/BiOBr can be collected from the treated aqueous solution conveniently and fast by applying an external magnetic field. Although the degradation efficiency of m-Fe_3O_4/BiOBr MSs is slightly decreased after each cycle, the m-Fe_3O_4/BiOBr MSs exhibited 82.78% activity in the third use under the simulated solar light irradiation. By contrast, the pure BiOBr showed a significant reduction in its photocatalytic degradation activity, which already decreased to 36.25% in the third use. The results indicate that m-Fe_3O_4/BiOBr MSs are more stable and recyclable for the photocatalytic removal of pollutant molecules. The possible reason for the obvious improvement of m-Fe_3O_4/BiOBr MSs is firstly that the introduction of Fe_3O_4 can facilitate the electron transfer of BiOBr, which promoted the effective separation of photoexcited electron-hole pairs. In addition, the presence Fe_3O_4 in m-Fe_3O_4/BiOBr MSs is advantageous to enhance the recovery rate of nanosized m-Fe_3O_4/BiOBr MSs by reducing the loss of the photocatalyst. Hence, it can be concluded that m-Fe_3O_4/BiOBr MSs can facilitate the practical running of an industrial wastewater treatment.

Radical trapping experiments

Generally, the reactive species, such as hydroxyl radicals ($^{\bullet}OH$), superoxide radical anions ($O_2^{-\bullet}$), and holes (h^+) are expected to be involved in the photocatalytic degradation of organic pollutants (Mehraj *et al.*, 2015). To investigate the role of main active species during photocatalytic reactivity, the radical and hole trapping experiments with different scavengers on the rate constant were carried out. N_2, ethylenediaminetetraaceticacid (EDTA) and tert-butanol (TBA) were added into CR dye solution to capture the hydroxyl radical ($^{\bullet}OH$), hole (h^+) and superoxide radical ($O_2^{-\bullet}$), respectively (Guo *et al.*, 2015). The more the reaction rate reduced the more important role the reactive species played in the photocatalytic reaction.

Taking account of decoloriaztion rate after 240 min under simulated solar irradiation, the trend of impeditive effect in the presence of different scavengers was as follows: EDTA > N_2 > TBA (Fig. 12). With the introduction of 1 mmol of EDTA as a hole scavenger, the kinetic rate of CR degradation was significantly decreased to 0.00252 min^{-1}, suggesting that h^+ plays a crucial role in CR degradation by m-Fe_3O_4/BiOBr MSs. The decreases of kinetic rate result from the fact that it is insufficient for the photogenerated valence band hole of BiOBr to oxidize water to $^{\bullet}OH$ (Zhang *et al.*, 2015a, 2015b). Meanwhile, the use of N_2 lowered the photocatalytic efficiency due to the reduction of active $^{\bullet}O_2^-$ because dissolved O_2 as an efficient electron scavenger was excluded by N_2 in the degradation process. Compared with

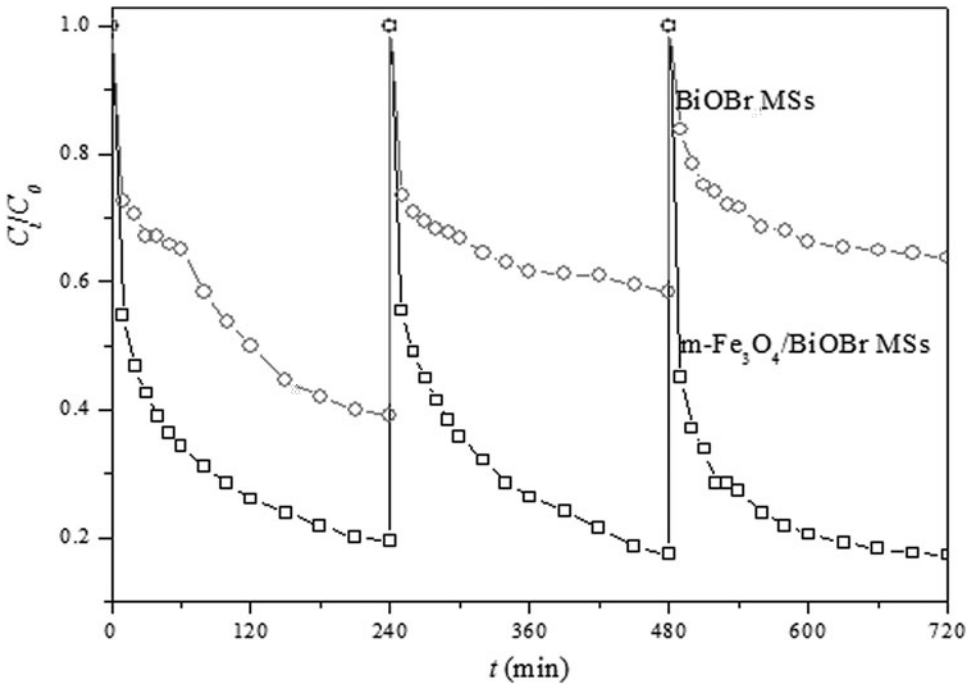

FIG. 11. Cycling runs of BiOBr MSs and m-Fe_3O_4/BiOBr MSs for the degradation of CR solution under simulated solar light.

the degradation system that does not contain any scavenger, the rates demonstrate that both the hole and $^{\bullet}O_2^-$ radicals are the main active species. However, with the addition of 1 mM of TBA as hydroxyl radicals scavenger, the change in degradation of CR indicated that hydroxyl radicals are one of the active species responding to CR degradation. Both the h^+ radicals and $O_2^{\bullet-}$ radicals were the two main active species that drive the photocatalytic decolorization of CR solution by m-Fe_3O_4/BiOBr MSs.

The photocatalytic mechanism of m-Fe_3O_4/BiOBr MSs for CR degradation under simulated solar light is illustrated in Fig. 13. First, when m-Fe_3O_4/BiOBr MSs are exposed to simulated solar light irradiation, the BiOBr MSs produced electrons and holes [Eq. (3)]. The electrons (e^-) on conduction band (CB) of the BiOBr rapidly transferred to Fe_3O_4 because the CB level of Fe_3O_4 (1.00 eV vs. Normal Hydrogen Electrode [NHE]) is much lower than that of BiOBr (0.59 V vs. NHE) and the good electrical conductivity of Fe_3O_4 is as high as 1.9×10^6 S/m (Zhu *et al.*, 2012; Liu *et al.*, 2015) [Eq. (4)]. Next, the migrated e^- reacted with the oxygen molecule (O_2) that dissolved in aqueous solution to generate $O_2^{\bullet-}$ [Eq. (5)]. Meanwhile, Fe_3O_4 nanoparticles on the surface of BiOBr can act as an electron capturer to improve the separation efficiency of the charge carriers and thereby

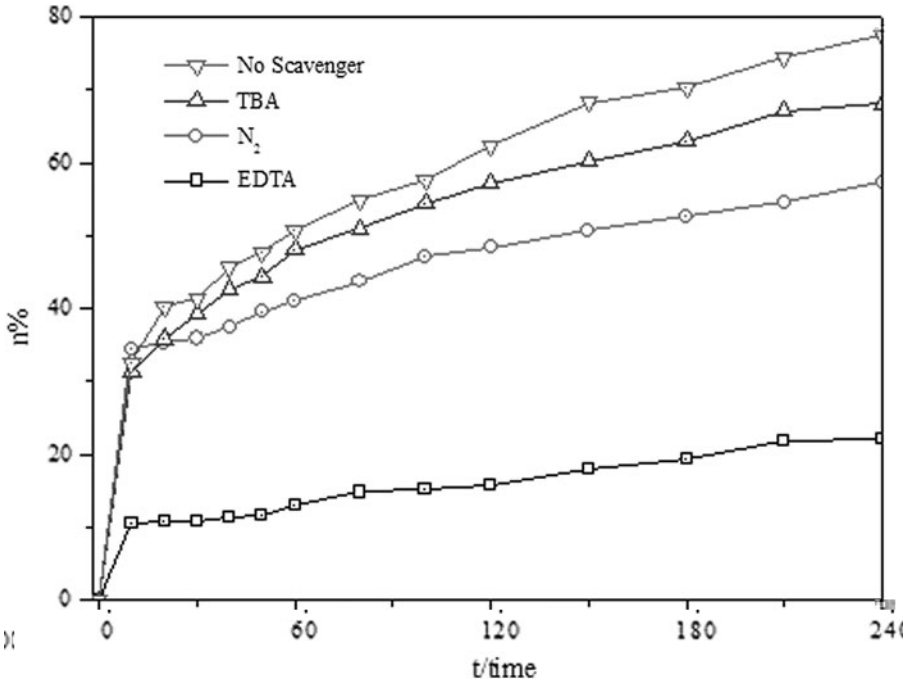

FIG. 12. Effect of radical scavengers on the photodegradation of CR on m-Fe_3O_4/BiOBr MSs.

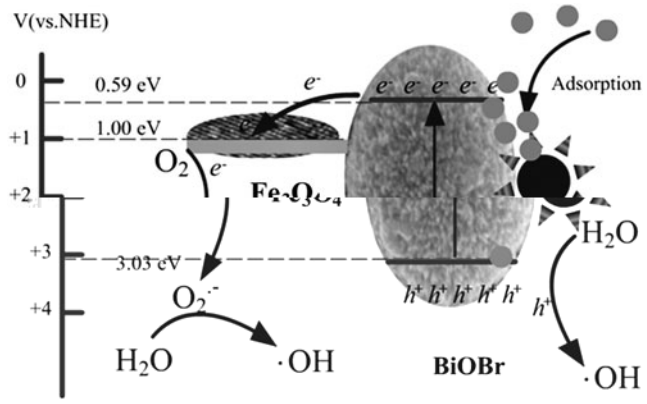

FIG. 13. Photocatalytic mechanism of CR degradation on m-Fe_3O_4/BiOBr MSs under simulated solar light irradiation.

improving the photocatalytic efficiency. These should be the main reason for the enhancement of the photocatalytic activity for m-Fe_3O_4/BiOBr MSs [Eq. (6)].

$$\text{BiOBr} + h\nu \rightarrow \text{BiOBr}(e_{CB}^{-}) + \text{BiOBr}(h_{VB}^{+}) \quad (3)$$

$$\text{BiOBr}(e_{CB}^{-}) + Fe_3O_4 \rightarrow \text{BiOBr} + Fe_3O_4(e_{CB}^{-}) \quad (4)$$

$$Fe_3O_4(e_{CB}^{-}) + O_2 \rightarrow O_2^{\cdot-} + Fe_3O_4 \quad (5)$$

$$\text{CR} + \text{reactive species}(O_2^{\cdot-}, {}^{\cdot}OH\ldots) \rightarrow CO_2 + H_2O + \text{other byproducts} \quad (6)$$

Conclusions

Recyclable m-Fe_3O_4/BiOBr MSs were synthesized by anchoring magnetic Fe_3O_4 nanoparticles to BiOBr MSs. These m-Fe_3O_4/BiOBr MSs displayed more effective photocatalytic activity than BiOBr MSs, which resulted from superior adsorption and transfer performance to organic contaminants in aqueous systems. The pseudo-first-order rate constants for photocatalytic degradation of CR were $0.0011\,min^{-1}$ and $0.0046\,min^{-1}$ using pure BiOBr and m-Fe_3O_4/BiOBr MSs, respectively. Both the h^+ radicals and $O_2^{\cdot-}$ radicals were the two main active species that drive the photocatalytic decolorization of CR solution by m-Fe_3O_4/BiOBr MSs under simulated solar light irradiation. The m-Fe_3O_4/BiOBr MSs can be easily recovered by an external magnet and redispersed after the treatment process. This work suggests that m-Fe_3O_4/BiOBr MSs may be a promising photocatalyst for photodegrading organic dye pollutants and environmental remediation.

Acknowledgments

The authors acknowledge the support of the Zhejiang Provincial Natural Science Foundation of China (LY15E080002 and LY15E020002), the Natural Science Foundation of China (Grant No. 51208331 and 51502188) and the Scientific and Technological Development Project of Taizhou City (Grant No. 1701hb02).

Author Disclosure Statement

No competing financial interests exist.

References

Ahmed, S., Rasul, M.G., Martens, W.N., Brown, R., and Hashib, M.A. (2011). Advances in heterogeneous photocatalytic degradation of phenols and dyes in wastewater: A review. *Water Air Soil Pollut*. 215, 3.

An, W., Cui, W., Liang, Y., Hu, J., and Liu, L. (2015). Surface decoration of $BiPO_4$ with BiOBr nanoflakes to build heterostructure photocatalysts with enhanced photocatalytic activity. *Appl. Surf. Sci*. 351, 1131.

Brillas, E., and Martínez-Huitle, C.A. (2015). Decontamination of wastewaters containing synthetic organic dyes by electrochemical methods. An updated review. *Appl. Catal. B Environ.* 166, 603.

Cao, C., Xiao, L., Chen, C., and Cao, Q. (2015). Magnetically separable Cu_2O/chitosan–Fe_3O_4 nanocomposites: Preparation, characterization and visible-light photocatalytic performance. *Appl. Surf. Sci*. 333, 110.

Chen, Y., Wen, M., and Wu, Q. (2011). Stepwise blossoming of BiOBr nanoplate-assembled microflowers and their visible-light photocatalytic activities. *Cryst. Eng. Comm*. 13, 3035.

Cheng, L., Zhang, S., Wang, Y., Ding, G., and Jiao, Z. (2016). Ternary P25–graphene–Fe_3O_4 nanocomposite as a magnetically recyclable hybrid for photodegradation of dyes. *Mater. Res. Bull*. 73, 77.

Gao, S., Guo, C., Lv, J., Wang, Q., Zhang, Y., Hou, S., Gao, J., and Xu, J. (2017). A novel 3D hollow magnetic Fe_3O_4/BiOI heterojunction with enhanced photocatalytic performance for bisphenol A degradation. *Chem. Eng. J*. 307, 1055.

Guo, Y., Huang, H., He, Y., Tian, N., Zhang, T., Chu, P.K., An, Q., and Zhang, Y. (2015). In situ crystallization for fabrication of core-satellites structured BiOBr-CdS heterostructure with an excellent visible–light–responsive photoreactivity. *Nanoscale* 7, 11702.

He, Q., Zhang, Z., Xiong, J., Xiong, Y., and Xiao, H. (2008). A novel biomaterial—Fe_3O_4:TiO_2 core-shell nano particle with magnetic performance and high visible light photocatalytic activity. *Opt. Mater*. 31, 380.

Huo, Y., Xie, Z., Wang, X., Li, H., Hoang, M., and Caruso, R.A. (2013). Methyl orange removal by combined visible-light photocatalysis and membrane distillation. *Dyes Pigments* 98, 106.

Huo, Y., Zhang, J., Miao, M., and Jin, Y. (2012). Solvothermal synthesis of flower-like BiOBr microspheres with highly visible-light photocatalytic performances. *Appl. Catal. B Environ*. 111, 334.

Idris, A.M., Shinger, M.I., Qin, D.D., Baballa, H., and Lu, X. (2014). An in-situ anion exchange method synthesized of Ag_3PO_4 functionalized with Fe_3O_4 and AgI for photocatalytic degradation of methyl orange under visible light irradiation. *Int. J. Mater. Sci. Appl*. 3, 303.

Jiang, R., Zhu, H.Y., Chen, H.H., Yao, J., Fu, Y.Q., Zhang, Z.Y., and Xu, Y.M. (2014). Effect of calcination temperature on physical parameters and photocatalytic activity of mesoporous titania spheres using chitosan/poly(vinyl alcohol) hydrogel beads as a template. *Appl. Surf. Sci.* 319, 189.

Jiang, R., Zhu, H.Y., Li, J.B., Fu, Y.Q., Yao, J., Jiang, S.T., and Zeng, G.M. (2016). Fabrication of novel magnetically separable BiOBr/$CoFe_2O_4$ microspheres and its application in the efficient removal of dye from aqueous phase by an environment-friendly and economical approach. *Appl. Surf. Sci*. 364, 604.

Lee, K.M., Lai, C.W., Ngai, K.S., and Juan, J.C., (2016). Recent developments of zinc oxide based photocatalyst in water treatment technology: A review. *Water Res.* 88, 428.

Li, C., Tan, J., Fan, X., Zhang, B., Zhang, H., and Zhang, Q. (2015). Magnetically separable one dimensional Fe_3O_4/P(MAA-DVB)/TiO_2 nanochains: Preparation, characterization and photocatalytic activity. *Ceram. Int*. 41, 3860.

Li, H., Liu, J., Hu, T., Du, N., and Hou, W. (2016). Synthesis of belt-like BiOBr hierarchical nanostructure with high photocatalytic performance. *Mater. Res. Bull*. 77, 171.

Lin, T., Wang, J., Guo, L., and Fu, F. (2015). Fe_3O_4@MoS_2 core–shell composites: Preparation, characterization, and catalytic application. *J. Phys. Chem. C* 119, 13658.

Linley, S., Leshuk, T., and Gu, F.X. (2013). Magnetically separable water treatment technologies and their role in future advanced water treatment: A patent review. *Clean Soil Air Water* 41, 1152.

Liu, Z.S., Wu, B.T., Niu, J.N., Feng, P.Z., and Zhu, Y.B. (2015). $BiPO_4$/BiOBr p–n junction photocatalysts: One-pot synthesis and dramatic visible light photocatalytic activity. *Mater. Res. Bull*. 63, 187.

Mehraj, O., Niyaz, A.M., Pirzada, B.M., and Sabir, S. (2015). Fabrication of novel Ag_3PO_4/BiOBr heterojunction with high stability and enhanced visible-light-driven photocatalytic activity. *Appl. Surf. Sci*. 332, 419.

Mera, A.C., Váldes, H., Jamett, F.J., and Meléndrez, M.F. (2017). BiOBr microspheres for photocatalytic degradation of an anionic dye. *Solid State Sci*. 65, 15.

Panthi, G., Park, M., Kim, H.-Y., Lee, S.-Y., and Park, S.-J. (2015). Electrospun ZnO hybrid nanofibers for photodegradation of wastewater containing organic dyes: A review. *J. Ind. Eng. Chem.* 21, 26.

Polshettiwar, V., Luque, R., Fihri, A., Zhu, H., Bouhrara, M., and Basset, J.M. (2011). Magnetically recoverable nanocatalysts. *Chem. Rev*. 111, 3036.

Reza, K.M., Kurny, A.S.W., and Gulshan, F. (2017). Parameters affecting the photocatalytic degradation of dyes using TiO_2: A review. *Appl. Water Sci.* 7, 1569.

Si, Y., Zhong, J., Li, J., Li, M., Yang, L., and Ding, J. (2016). Efficient solar-driven photocatalytic performance of BiOBr benefiting from enhanced charge separation rate. *Mater. Lett*. 163, 175.

Wei, X.X., Cui, H.T., Guo, S.Q., Zhao, L.F., and Li, W. (2013). Hybrid BiOBr–TiO_2 nanocomposites with high visible light photocatalytic activity for water treatment. *J. Hazard. Mater*. 263, 650.

Wen, S., Gao, B., Xu, X., Xing, L., Han, S., Duan, P., Song, W., and Jia, R. (2016). Adsorption–desorption behavior of magnetic amine/Fe_3O_4 functionalized biopolymer resin towards anionic dyes from wastewater. *Bioresour. Technol*. 210, 123.

Xue, C., Xia, J., Wang, T., Zhao, S., Yang, G., Yang, B., Dai, Y., and Yang, G. (2014). A facile and efficient solvothermal fabrication of three-dimensionally hierarchical BiOBr microspheres with exceptional photocatalytic activity. *Mater. Lett*. 133, 274.

Yu, C., Cao, F., Li, G., Wei, R., Yu, J.C., Jin, R., Fan, Q., and Wang, C. (2013). Novel noble metal (Rh, Pd, Pt)/BiOX(Cl, Br, I) composite photocatalysts with enhanced photocatalytic performance in dye degradation. *Sep. Purif. Technol*. 120, 110.

Zhang, W., Jia, B., Wang, Q., and Dionysiou, D. (2015a). Visible-light sensitization of TiO_2 photocatalysts via wet chemical N-doping for the degradation of dissolved organic compounds in wastewater treatment: A review. *J. Nanopart. Res.* 17, 221.

Zhang, X., Li, R., Jia, M., Wang, S., Huang, Y., and Chen, C. (2015b). Degradation of ciprofloxacin in aqueous bismuth oxybromide (BiOBr) suspensions under visible light irradiation: A direct hole oxidation pathway. *Chem. Eng. J*. 274, 290.

Zhao, Y., Tan, X., Yu, T., and Wang, S. (2016). SDS-assisted solvothermal synthesis of BiOBr microspheres with highly visible-light photocatalytic activity. *Mater. Lett*. 164, 243.

Zhi, J., Wang, Y., Lu, Y., Ma, J., and Luo, G. (2006). In situ preparation of magnetic chitosan/Fe_3O_4 composite nanoparticles in tiny pools of water-in-oil microemulsion. *React. Funct. Polym*. 66, 1552.

Zhi, Z., Lu, Z., Wang, D., Tang, X., Yana, Y., Shi, W., Wang, Y., Gao, N., Yao, X., and Dong, H. (2016). Construction of high-dispersed Ag/Fe_3O_4/g-C_3N_4 photocatalyst byselective photo-deposition and improved photocatalytic activity. *Appl. Catal. B Environ*. 182, 115.

Zhu, H.Y., Fu, Y.Q., Jiang, R., Jiang, J.H., Xiao, L., Zeng, G.M., Zhao, S.L., and Wang, Y. (2011). Adsorption removal of Congo red onto magnetic cellulose/Fe_3O_4/activated carbon composite: Equilibrium, kinetic and thermodynamic studies. *Chem. Eng. J.* 173, 494.

Zhu, H.Y., Jiang, R., Fu, Y.Q., Guan, Y.J., Yao, J., Xiao, L., and Zeng, G.M. (2012). Effective photocatalytic decolorization of methyl orange utilizing TiO_2/ZnO/chitosan nanocomposite films under simulated solar irradiation. *Desalination* 286, 41.

Zhu, H.Y., Jiang, R., Fu, Y.Q., Li, R.R., Yao, J., and Jiang, S.T. (2016). Novel multifunctional $N_iFe_2O_4$/ZnO hybrids for dye removal by adsorption, photocatalysis and magnetic separation. *Appl. Surf. Sci*. 369, 1.

Zhu, H.Y., Jiang, R., Li, J.B., Fu, Y.Q., Jiang, S.T., and Yao, J. (2017). Magnetically recyclable Fe_3O_4/Bi_2S_3 microspheres for effective removal of Congo red dye by simultaneous adsorption and photocatalytic regeneration. *Sep. Purif. Technol*. 179, 184.

Zhu, H.Y., Jiang, R, Xiao, L., Chang, Y.H., Guan, Y.J., Li, X.D., and Zeng, G.M. (2009). Photocatalytic decolorization and degradation of Congo red on innovative crosslinked chitosan/nano-CdS composite catalyst under visible light irradiation. *J. Hazard. Mater*. 169, 933.